



**EUROfusion**

WPS1-PR(18) 21092

TS Pedersen et al.

## **First results from divertor operation in Wendelstein 7-X**

Preprint of Paper to be submitted for publication in  
Plasma Physics and Controlled Fusion



This work has been carried out within the framework of the EUROfusion Consortium and has received funding from the Euratom research and training programme 2014-2018 under grant agreement No 633053. The views and opinions expressed herein do not necessarily reflect those of the European Commission.

This document is intended for publication in the open literature. It is made available on the clear understanding that it may not be further circulated and extracts or references may not be published prior to publication of the original when applicable, or without the consent of the Publications Officer, EUROfusion Programme Management Unit, Culham Science Centre, Abingdon, Oxon, OX14 3DB, UK or e-mail [Publications.Officer@euro-fusion.org](mailto:Publications.Officer@euro-fusion.org)

Enquiries about Copyright and reproduction should be addressed to the Publications Officer, EUROfusion Programme Management Unit, Culham Science Centre, Abingdon, Oxon, OX14 3DB, UK or e-mail [Publications.Officer@euro-fusion.org](mailto:Publications.Officer@euro-fusion.org)

The contents of this preprint and all other EUROfusion Preprints, Reports and Conference Papers are available to view online free at <http://www.euro-fusionscipub.org>. This site has full search facilities and e-mail alert options. In the JET specific papers the diagrams contained within the PDFs on this site are hyperlinked

# First results from divertor operation in Wendelstein 7-X

Thomas Sunn Pedersen,<sup>\*</sup> Ralf König, Maciej Krychowiak, Jürgen Baldzuhn, Sergey Bozhenkov, Golo Fuchert, Andreas Langenberg, Marcin Jakubowski, Holger Niemann, Daihong Zhang, Kian Rahbarnia, Hans-Stephan Bosch, and the W7-X Team  
*Max Planck Institute for Plasma Physics, Greifswald, Germany*

Yevgen Kazakov  
*Laboratory for Plasma Physics, LPP-ERM/KMS, Brussels, Belgium*

Yu Gao  
*Research Center Jülich, Jülich, Germany*

Novimir Pablant  
*Princeton Plasma Physics Laboratory, Princeton, NJ 08543, USA*

(Dated: September 6, 2018)

## Abstract

Wendelstein 7-X (W7-X) is a highly optimized stellarator experiment that went into operation in 2015. With a 30 cubic meter volume, a superconducting coil system operating at 2.5 T, and steady-state heating capability of eventually up to 10 MW, it was built to demonstrate the benefits of optimized stellarators at parameters approaching those of a fusion power plant. We report here on the first results with the test-divertor installed, during the second operation phase (OP1.2a), which was performed in the second half of 2017. Operation with a divertor, and the addition of several new fueling systems allowed higher density operation in hydrogen as well as helium. The effects that higher density operation had on both divertor operation and global confinement will be described. In particular, at high densities detachment was observed, and the highest fusion triple product for a stellarator was achieved.

---

<sup>\*</sup> [tspe@ipp.mpg.de](mailto:tspe@ipp.mpg.de)

## I. INTRODUCTION

The Wendelstein 7-X (W7-X) experiment [1] is the most advanced stellarator in the world today. It went into operation in 2015 with a minimal setup of its plasma-facing components, most notably, five discrete graphite limiters mounted on the inboard side in the narrow (bean-shaped) cross-sections. With this simplified setup, it was possible to run plasmas with pulse energies up to 4 MJ, pulse lengths up to 6 seconds, and triple products up to  $0.08 \times 10^{20}$  keV m<sup>-3</sup> sec., [2], allowing a rather comprehensive first set of physics studies (see eg. [3, 4, 6, 7], including the first verification of the W7-X optimization, the control and near-elimination of the toroidal bootstrap current [8]. However, it was always foreseen for W7-X to use the island divertor concept, first in use in W7-AS (see eg. [5]). This paper describes some of the most important first results from operation with the test divertor units (TDU), the operation phase 1.2a (OP1.2a).

## II. GOALS AND FEATURES OF THE OPERATION PHASE 1.2A

OP1.2a was performed in the second half of 2017. As described in earlier publications about W7-X (see eg. [2]), and discussed again here in Sections III and IV, a credible path to higher performance in W7-X is a significant increase in plasma density and a commensurate increase in heating power, and OP1.2a indeed featured upgrades that allowed both density and power increases, the most important ones summarized in the following.

Most prominently, OP1.2a featured a much expanded set of plasma-facing components, including a test divertor (Section V), allowing for better particle exhaust but also a much larger area of plasma-facing surface, and thereby a much higher injected heating energy per pulse (80 MJ, as compared to 4 MJ at the end of OP1.1), and a better separation between the plasma-wall interaction region and the core plasma than in the OP1.1 limiter operation. Also, two new fueling systems were taken into operation, pellet injection (Section VII) and a divertor gas injection system (Section IX). As discussed in Section IV, there are empirical limits to the achievable density in stellarators stemming from power balance, so an increase in heating power is not only needed for performance extension, it might well be necessary for the desired density increases. The ECRH heating capabilities were indeed expanded from six gyrotrons and a maximum achieved heating power into the plasma of 4.3 MW in OP1.1,

to ten gyrotrons, and a maximum achieved 7 MW of heating in OP1.2a [9]. Another important ingredient for reaching high densities stably in fusion devices is wall-conditioning. In OP1.1, only relatively short glow-discharge cleaning discharges were performed. The limitation was out of concern that the many CuCrZr heat shield structures, which were left bare in OP1.1, would cause excess sputtering of especially copper onto the graphite limiters. In OP1.2a, all CuCrZr structures were covered with their foreseen graphite tiles, and much longer glow-discharge cleaning (GDC) in both hydrogen and helium was safely performed. ECRH conditioning with helium plasmas was also extensively used (as was already the case in OP1.1), but for logistical reasons, it was not possible to perform boronization in OP1.2a. Nevertheless, the GDC and ECRH wall-conditioning resulted in wall outgassing being lower after two weeks of operation in OP1.2a than it had been even at the end of the three month period of OP1.1 [10].

### III. HIGHER TRIPLE PRODUCTS THROUGH HIGHER DENSITY

The triple product ( $n_i T_i \tau_E$ ) is an important figure of merit towards the creation of net energy using the D-T fusion reaction [11], and is useful when comparing different fusion concepts. The energy confinement time  $\tau_E$  has been difficult to predict from first principles, and although much progress has been made on this front, empirical scalings are still in widespread use. The ISS04 scaling [12] is such a scaling for stellarator plasmas, which can also be applied to tokamak plasmas. It is expressed in terms of parameters that are, or generally can assumed to be, determined by the experimenter while designing or operating the device: Plasma major radius ( $R$ , in meters), minor radius ( $a$ , in meters), magnetic field strength on the magnetic axis ( $B$ , in Tesla), the magnetic winding number iota at  $r/a = 2/3$  ( $\iota = 1/q$ , with  $q$  the tokamak safety factor), the applied heating power ( $P$ , in megawatts) and the line-averaged electron density  $n_e$ , in units of  $10^{20} \text{ m}^{-3}$ , and  $\tau_E$  in seconds:

$$\tau_E = 0.134 a^{2.28} R^{0.64} P^{-0.61} n_e^{0.54} B^{0.84} \iota^{0.41} \quad (1)$$

To guide our thinking in the following discussion, we approximate the ISS04 scaling by this somewhat simpler expression:

$$\tau_E \propto V B \iota^{0.4} (n_e/P)^{0.6} \quad (2)$$

It is seen that increasing the plasma volume ( $V$ ) and the magnetic field ( $B$ ) will increase the confinement time (approximately linearly). For an already constructed experiment, such as W7-X, there are upper limits to  $B$  and  $V$ . In W7-X, for reasons related to the vessel shape and the island divertor,  $\iota$  can only be varied in a rather restricted range from  $\iota \approx 0.8$  to 1.25, as also discussed in Section V. Given the relatively small exponent, 0.41,  $\iota$  is expected to play an interesting but minor role for the optimization of the confinement and the triple product in W7-X. The heating power  $P$  and density  $n_e$  can be varied over at least an order of magnitude, however. We therefore analyze in the following how these two parameters affect the triple product. We assume that the ISS04 scaling holds, that  $T_e = T_i \equiv T$  and that  $n_e = n_i \equiv n$ , since these relations are expected to be good approximations at high densities in W7-X, and also are relevant for a reactor. We will restrict this analysis to pressure values below the  $\beta$  limits of W7-X [13].

The plasma thermal energy density is then  $3nT$ . Therefore,  $nT$  is proportional to the total plasma energy (ignoring profile changes) which then scales as  $P \times \tau_E$ . Therefore, the triple product  $nT\tau_E$  scales as  $P \times \tau_E^2 \propto P^{-0.2}n^{1.2}$  using our approximate version, or  $P^{-0.22}n^{1.08}$  when using the actual ISS04 coefficients. One sees that increasing the density alone (ie. keeping the other components constant) increases the triple product slightly faster than linearly, whereas increasing heating power has a slightly negative effect. The second conclusion is potentially misleading since it appears to say that heating power is not important for reaching high triple products, which is not true, for two reasons. One reason is that the particular importance of the triple product as *the* figure of merit for D-T fusion only holds in the  $T=10-40$  keV range, whereas for  $T < 10$  keV, the D-T fusion cross section falls off faster than  $T^2$ . The second reason is that density cannot be increased arbitrarily: a certain amount of heating power is needed to prevent the plasma from a radiative collapse at low temperature. In the following, we discuss this, in the broader context of density limits.

#### IV. DENSITY LIMITS IN STELLARATORS AND TOKAMAKS

Since a density increase is an efficient way to increase the triple product, it is an important advantage of stellarators that they are not subject to a Greenwald-like density limit. The Greenwald density limit in its original form [14] is  $n_G = I_p/(\pi a^2)$ , with  $n_G$  in units of

$10^{20}\text{m}^{-3}$ ,  $I_p$  the toroidal plasma-current in mega-ampere, and  $a$  (plasma minor radius) in meters. Since stellarators in general, and W7-X in particular [8], have much lower toroidal currents than equivalent-size tokamaks, they would appear to have a very low Greenwald density limit. To understand the relevance of the Greenwald limit, and how it should be extended to stellarators, we recast it in terms of a density limit that scales with the confining toroidal magnetic field. This connection is not new, but we have been unable to find a reference that provides a simple derivation of this. The tokamak connection between maximum parallel plasma current and toroidal magnetic field comes from magnetohydrodynamics (MHD) stability. Quoted from Troyon et al. speaking about tokamak stability [15]: "The current is limited to a value corresponding to a safety factor slightly above 2 at the plasma surface." For a circular-cross-section tokamak, Troyon's statement  $q_a > 2$  is equivalent to

$$I_p < \frac{\pi a^2}{\mu_0 R} B_t \quad (3)$$

For a given toroidal B-field, the tokamak Greenwald density limit is therefore:

$$n < n_G = k \frac{I_p}{\pi a^2} < k \frac{\pi a^2}{\mu_0 R} B_t \frac{1}{\pi a^2} = k \frac{B_t}{\mu_0 R} \quad (4)$$

where the factor of  $k = 10^{14}$  is needed to convert into SI units or  $k = 10^{-6}$  if measuring the density in units of  $10^{20} \text{ m}^{-3}$ . A convenient version of this equation is then  $n_G = 0.80 \times B_t/R$ , with  $n_G$  in units of  $10^{20} \text{ m}^{-3}$ ,  $B_t$  in Tesla, and  $R$  in meters. The magnetic field strength has engineering limits, and, apart from major radius, the Greenwald density limit does not depend on anything else (importantly, not heating power). For current-generation superconductors (NbSn, NbTi) the values of  $n_G$  for fusion reactor designs are below those that would otherwise be optimal for a burning plasma. If W7-X ( $R=5.5 \text{ m}$ ,  $B=2.5 \text{ T}$ ), were subject to this density limit, the achievable density would be only  $0.36 \times 10^{20} \text{ m}^{-3}$ . This limit has been exceeded by more than a factor of two already in W7-X (see an example in Section X), and the limit has been exceeded by more than a factor of 10 in LHD [16].

However, a different and more benign density limit for stellarators has been observed. It is related to power balance, and an empirical formula for it was first published by Sudo [17]:

$$n_{20} < 0.25 \sqrt{\frac{PB}{a^2 R}} \quad (5)$$

Here  $n_{20}$  is the average density in units of  $10^{20} \text{ m}^{-3}$ ,  $P$  is in MW,  $a$  and  $R$  in meters and  $B$  in Tesla. Taking the plasma density to be at the Sudo limit, we now find that the triple

product scales as  $P^{0.32}$ , a positive but admittedly still rather weak scaling. The  $T > 10$  keV argument for a minimal heating power is the more important argument for having a minimal heating power. For a recent analysis of density limits in both tokamaks and stellarators, and their physical origins, we refer the reader to the paper by Zanca et al [18]. In the first operation phase of W7-X, OP1.1, a density limit was also observed [19], roughly but not entirely consistent with that of Sudo.

## V. THE TEST ISLAND DIVERTOR OF W7-X

### A. The interaction between the divertor plates and the island topology

As just discussed, stable, high density operation requires sufficient power, but efficient particle fueling and exhaust must also be implemented. In W7-X, the exhaust concept is that of the island divertor. For OP1.2a, ten identical uncooled graphite test divertor units (TDUs [20]) have been installed to handle the power and particle exhaust. The plasma-facing surfaces of these TDUs are identical to those of the later water-cooled carbon-fiber composite divertor, the high-heat flux (HHF) divertor [21]. The TDU allows first experience with island divertor operation and the specific geometry of the HHF divertor plates, and, since it cannot be significantly damaged even if the incident plasma heat flux is above 10 MW/m<sup>2</sup> (the design limit of the HHF divertor), this first exploration can occur even without protection interlock systems in full operation. The geometry of the divertor and the plasma shape is shown in Figure 1.. As can be seen, the ten TDUs are distributed according to the five-fold symmetry of the W7-X device, with each of the five modules containing one upper and one lower TDU.

Each TDU consists of a horizontal ( $\sim 1.86$  m<sup>2</sup>) and a vertical ( $\sim 0.55$  m<sup>2</sup>) divertor plate, separated by the pumping gap.

A low-shear multi-X-point island divertor concept [22] is realized by the interaction between large island chains at the plasma boundary, and the divertor plates.

W7-X has a five-fold symmetry, and a sizeable  $n=5$  (toroidal mode number) magnetic field component. The three island chains used for the island divertor are with edge rotational transform  $t_a = 5/m = 5/6$  (low iota configuration),  $5/5$  (standard and high mirror configuration), and  $5/4$  (high iota configuration), where  $m$  is the poloidal mode number. The



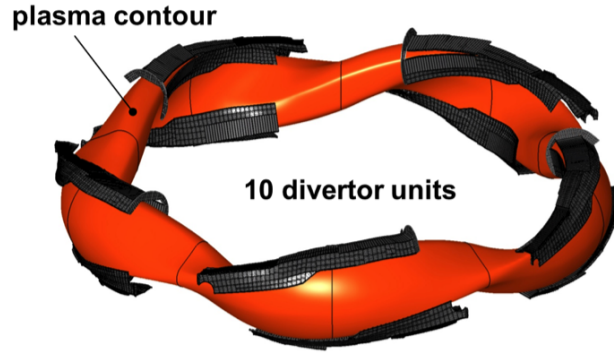


FIG. 1: This figure shows a CAD drawing of the ten test divertor units and the last closed flux surface.

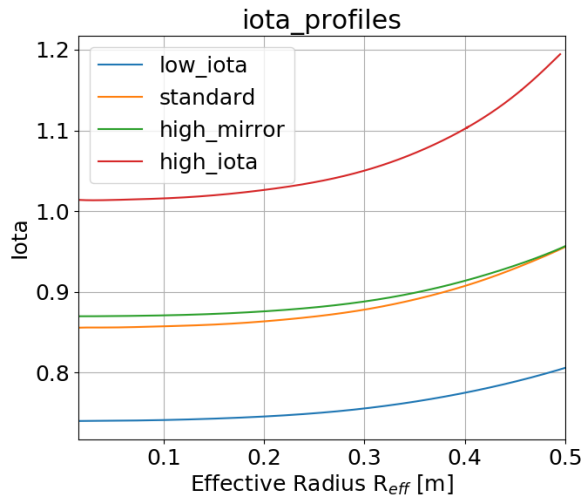


FIG. 2: The rotational transform profiles of different magnetic configurations in W7-X.

rotational transform profiles of these three configurations are shown in **Fig. 2**. The magnetic islands are intersected by the divertor plates. In this way, similar yet not identical to the tokamak x-point divertor, an indirect contact with the plasma is established: The plasma heat and particles flowing out of the closed magnetic surface diffuse into the interior of the island chain, and also across the x-points to the field lines just outside the island chain. The heat and particles are then led along these open field lines and deposited onto the target plates. This is illustrated in **Fig. 3**.

By separating the plasma-surface interaction region from the confinement region, the edge island is meant to prevent the core plasma from direct exposure to the recycling neutrals and the sputtered impurities.

**Fig. 4** summarizes the geometry of the intersected islands for the main magnetic con-

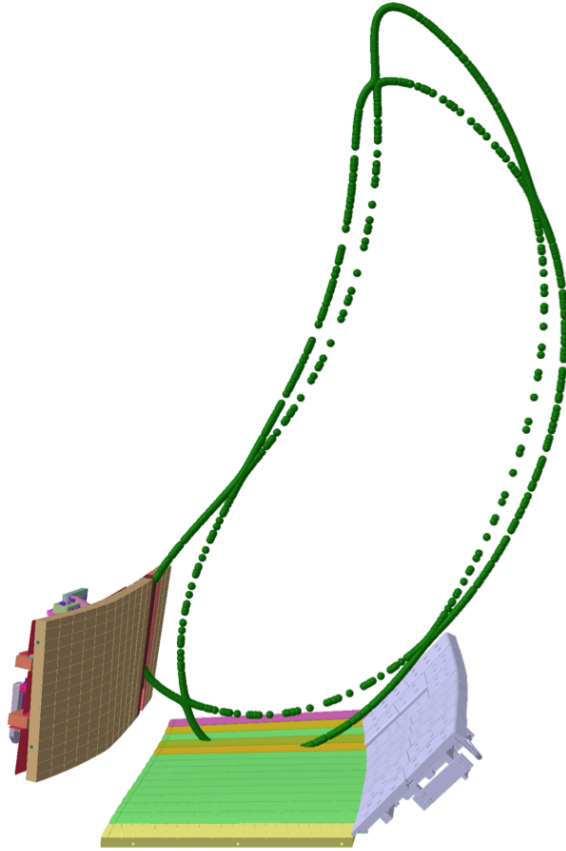


FIG. 3: The island divertor concept is illustrated by displaying a Poincaré cross section in a CAD model of a divertor unit in W7-X. The island chain allows some physical separation between the edge of the confinement region and the region where the outflowing plasma hits the divertor plate.

figurations, as well as the wall to wall connection length ( $L_c$ ) of the open field lines. The typical  $L_c$  in the island divertor in W7-X is about one order of magnitude longer than that in medium sized tokamak, which should lead to broader deposition patterns [2, 22].

Different magnetic configurations interact with different part of the divertor plates, resulting in different divertor footprints of heat loads, as simulated using diffusive field line tracing [23] in **Fig. 5**.

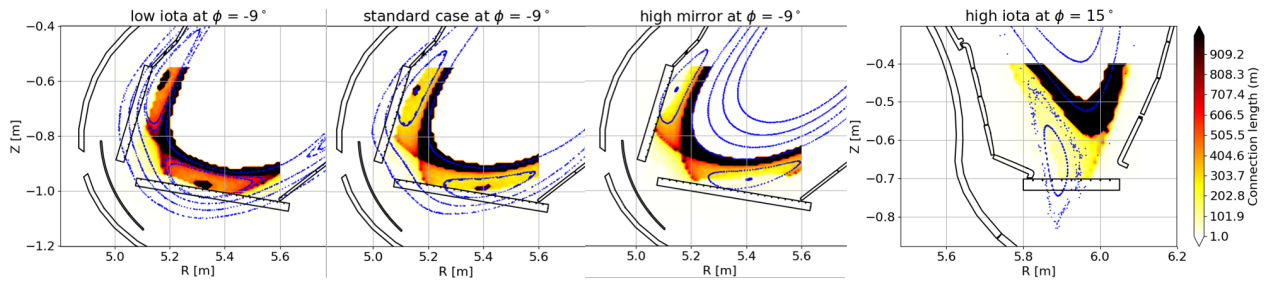


FIG. 4: The interaction between magnetic islands with the divertor plates under different magnetic configurations. The toroidal angle  $\phi$  is marked in blue in **Fig. 5**.

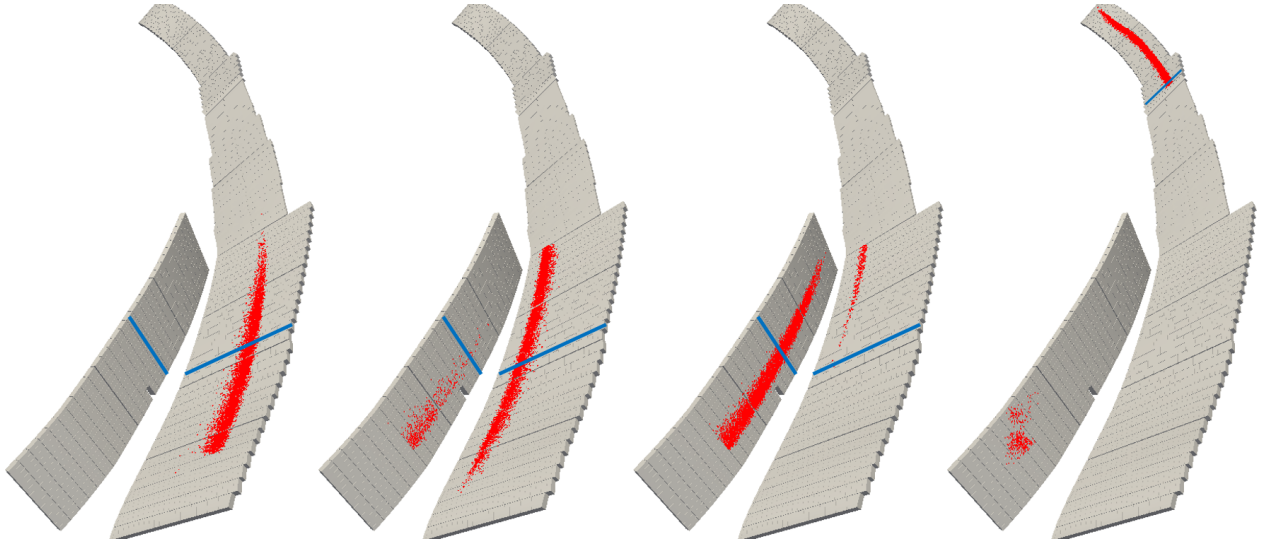


FIG. 5: The diffusive field line tracing simulation indicating the expected wetted area on the divertor plates for different magnetic configurations. From left to right: low iota, standard, high mirror and high iota configuration.

## VI. CHARACTERIZATION OF HEAT LOADS DURING ATTACHED OPERATION

The experimental strike-line patterns are shown in the following; they are in good agreement with our simulation results. Having verified a high accuracy of the magnetic field structure before operation started [24], the agreement of these heat load patterns is indirect evidence of the accuracy of the TDU installation. The experimental strike-line patterns were obtained using infrared camera systems to monitor the surface temperatures of the main plasma facing components [25]. Since Wendelstein 7-X has 10 discrete divertor modules, 10 observation systems instruments are required to provide full information on the power

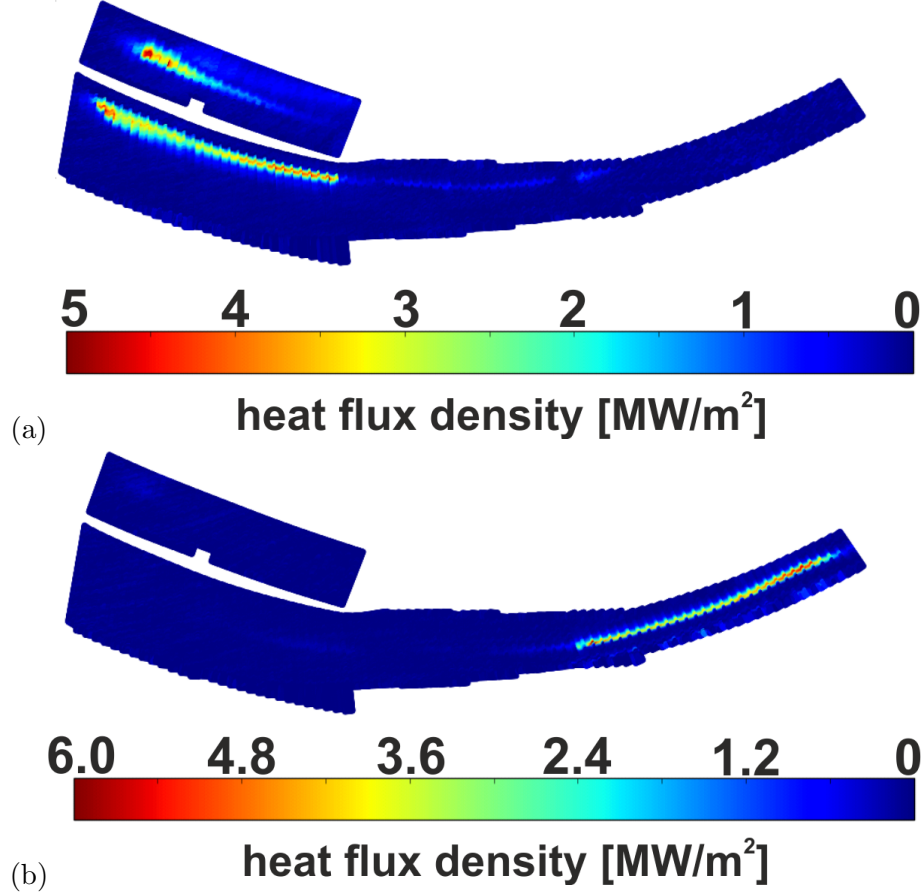


FIG. 6: Heat flux measured on the surface of one of the ten divertors of W7-X for (a) standard configuration (W7-X #20171108.015), to be compared with the second from the left subfigure in Figure 5, and (b) high-iota configuration (W7-X #20171025.030), to be compared with the rightmost subfigure in Fig. 5.

deposition onto the divertor. The surface temperature is measured by cameras with wavelength ranges 8-10  $\mu\text{m}$  or 3-5  $\mu\text{m}$ , and the heat flux is derived by solving the heat diffusion equation for the bulk of the tile with the the measured surface temperature evolution as an input parameter [26]. In OP1.2a, three different magnetic configurations were investigated: *standard*, *high-iota* and *high-mirror*. Examples for standard and high iota are presented in Fig. 6, showing the same general features as seen in Fig. 5. Both discharges were heated with 5 MW of ECRH power and had a line-averaged density of appr.  $2 \times 10^{19} \text{ [m}^{-3}\text{]}$ .

As the power load distribution depends strongly on the magnetic configuration, the measured wetted areas and peak heat fluxes are different for the different configurations. Maximum heat flux values of up to  $8 \text{ MW/m}^2$ , and strike-line widths of up to 11 cm were observed.

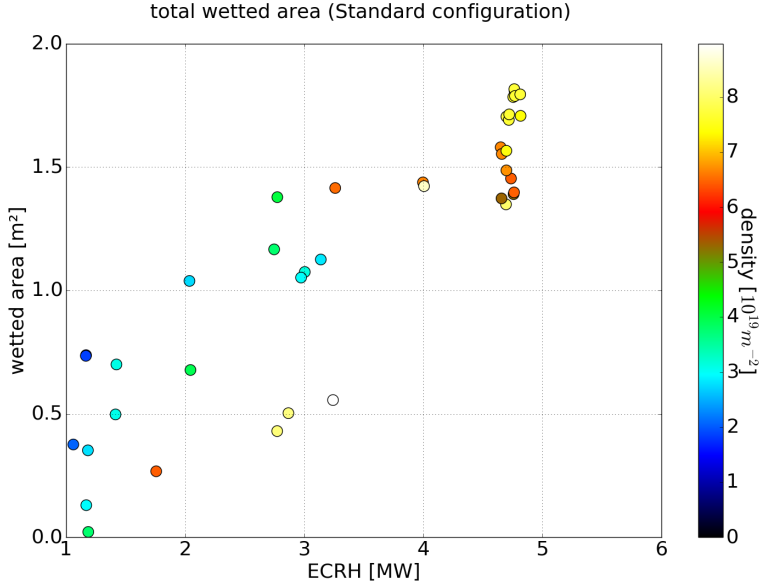


FIG. 7: The wetted area is shown as a function of heating power for the standard magnetic configuration. The wetted area goes up to above  $1.5 \text{ m}^2$  for high heating powers.

We characterize the heat-flux spreading in terms of the effective wetted area, which is defined as the equivalent area over which the maximum measured heat flux would extend to, so that it amounts to the total heat received by the divertor plates. In the standard configuration this increases as a function of heating power to approx.  $1.5 \text{ m}^2$  at  $P_{ECRH}=5 \text{ MW}$ . This is shown in Fig. 7 for the standard ( $t_a = 1$ ) configuration. Although extrapolations to even higher heating powers are bound to have large uncertainties, it is nonetheless a reassuring result. If the wetted area will increase linearly, the peak heat fluxes will be only about  $3.3 \text{ MW/m}^2$  for  $10 \text{ MW}$  reaching the divertor, and only  $6.7 \text{ MW/m}^2$  if the wetted area stays around  $1.5 \text{ m}^2$ . These numbers are well below the  $10 \text{ MW/m}^2$  limit for the HHF divertor during steady-state operation ( $P \leq 10 \text{ MW}$ ). By comparison, for ASDEX-Upgrade in L-mode, the wetted area is of order  $0.3 \text{ m}^2$  [27]).

## VII. FIRST OPERATION WITH PELLETT FUELING

For OP1.2a, a blower-gun pellet injector [28] was taken into operation. This injector allows for the injection of up to 60 hydrogen pellets within one plasma discharge, then new ice has to be generated. The pellets are accelerated by helium propellant gas to a speed of typically 200

m/s to 250 m/s. In comparison to gas puff injection from remote locations, pellet injection provided an unproblematic means to reach to high densities even in the plasma center. In particular in hydrogen plasma discharges, their rapid and efficient fueling helped to reach high densities, at least transiently, and this triggered then the first divertor detachment results, as described in the next section.

## VIII. OBSERVATIONS OF DETACHMENT

Stable and complete power detachment across all 10 discrete island divertors modules was observed for several seconds in hydrogen pellet fuelled discharges at 3 MW of ECRH heating and line averaged densities of  $2 \times 10^{19} \text{ m}^{-3}$ . At the transition into the detached phase, the local peak heat flux dropped from about  $5 \text{ MW/m}^2$  to below the detection limit of  $0.4 \text{ MW/m}^2$  of our infrared camera system, as shown in Fig. 8. This was observed with IR cameras that monitor all 10 discrete island divertors of W7-X. Complete detachment was found to have little effect on the measured energy confinement time, as evidenced by measurements of the plasma stored energy done with diamagnetic loops,  $W_{dia}$  [30], which was only about 10% lower at the end of the discharge than before the pellet injection at about the same density (fig. A). During the heat-flux detached phase, a highly radiative mantle was observed in the vicinity of the separatrix by the two nearly perpendicular oriented multi-channel bolometer systems covering the triangular shaped plane of the W7-X plasma. The two bolometer systems are located in the symmetry plane between two W7-X device modules, where no island divertor targets are installed. Throughout the stable completely detached phase, the total radiation fraction derived from the bolometer signals was always close to 100% [31], also shown here as part of fig. 8. Accurate total radiation values are difficult to derive from the measurements in just one single poloidal cross section of W7-X due to the 3D structure of the magnetic field.

The edge radiation during detachment is believed to be dominated by carbon and oxygen. The strongest evidence for oxygen comes from the observed one- to two-orders of magnitude increase of the CO level in the exhaust gas during these discharges. The steady increase of the uncooled divertor bulk target temperature throughout the day, up to sometimes  $400^\circ\text{C}$ , resulted in a steady increase in  $H_2O$  and  $CO$  base pressure by a factor of 10 between dis-

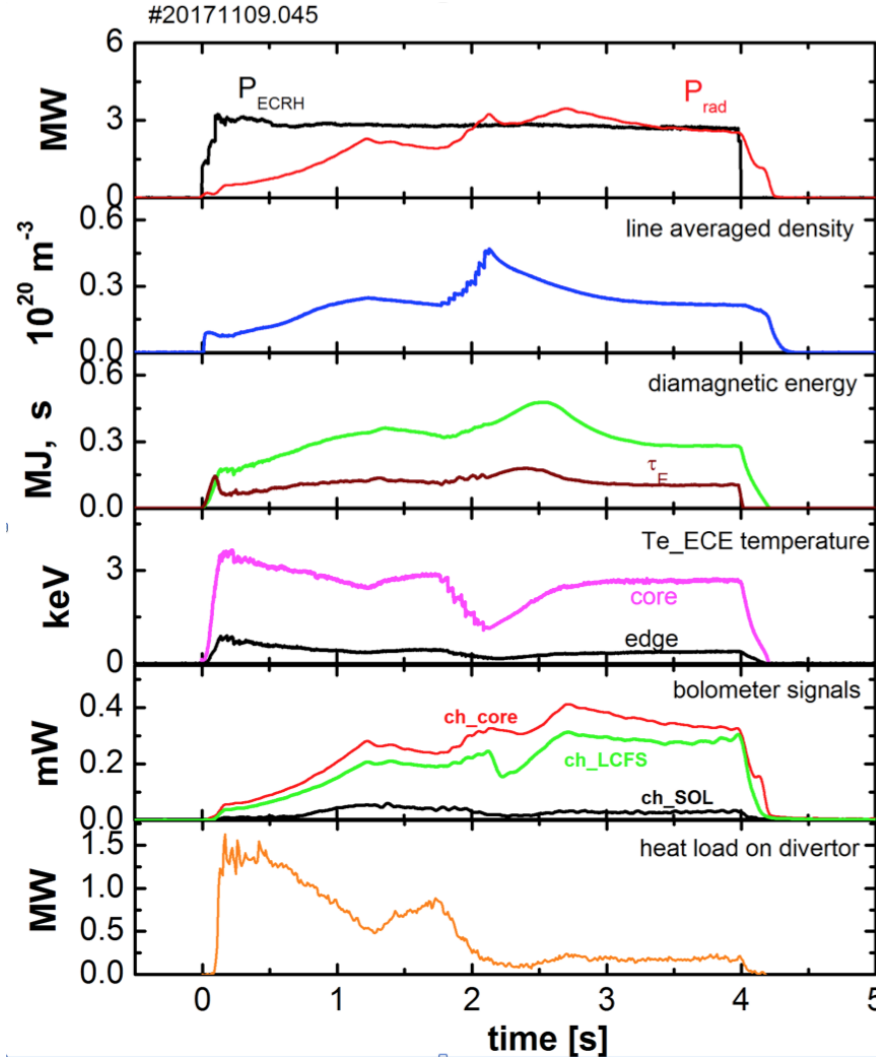


FIG. 8: An overview plot of a discharge where heat-flux detachment was observed. The line-averaged density was increased by pellet injection at a 30 Hz repetition rate from  $t=1.8$  s to  $t=2.3$  seconds. During this time, the divertor heat flux dropped down to less than  $0.3$  MW/m<sup>2</sup>, and, after pellet injection stopped, the plasma stayed detached, and the plasma confinement time remained at about  $0.1$  s for about one second, until the heating was terminated at  $t=4$  seconds.

charges, i.e. increased outgassing of water from the target tiles was constantly observed [32]. Boronisation was not yet available in OP1.2a, so to keep the oxygen at acceptable levels for maintaining operation, cleaning discharges in helium every two to three discharges was needed to maintain stable discharge conditions throughout the day. Indications for high recycling or the formation of a high-density recombining zone, as observed earlier on W7-AS

[33], were not found during the heat-flux detached phase.

## IX. FIRST HYDROGEN OPERATION OF THE DIVERTOR GAS INLET SYSTEM

For OP1.1 two gas injection vacuum plugins were installed and operated with non-explosive gases [34]. For OP1.2a the vacuum plugins were upgraded for operation with explosive gases. Each plugin consists of a box with five piezo-valves and four lines feeding the cooling water, the gasses and electrical cables from the vacuum flange to the gas valve box (Figure 9). The box is mounted at the backside of one of the horizontal divertor plates. Five capillary nozzles of 10 cm length end at the plasma-facing surface of the divertor and allow feeding the gases directly into the divertor plasma. One of the plugins is installed at the upper divertor in machine modules 51, the other at the bottom divertor in module 30.

This versatile gas injection system with its capability of a very wide range of reservoir pressure (from 2 mbar up to 60 bar) has a precise timing and short valve opening-times (down to 2 ms) and is used for various applications: tracer amounts of helium are used for measurement of  $n_e$  and  $T_e$  profiles in the magnetic island at the divertor plate [35]; neon is being investigated for potential extension of the measured parameter range towards lower temperatures and higher densities in the detached plasma conditions [36]; small argon puffs allow measurements of  $T_i$  and electrical fields in the plasma core in the x-ray wavelength-range, as well as impurity transport studies in the plasma core; Neon, nitrogen and methane are used for radiative edge cooling experiments [37] and studies of carbon erosion and transport [38]. Last but not least, hydrogen and helium were used for plasma fuelling and particle balance studies [39] and (in case of hydrogen) for triggering and control of plasma detachment from the divertor plates [40]. Effective fuelling of a hydrogen plasma was demonstrated in a standard divertor configuration with reversed field (see Fig. 10). The preprogrammed series of short hydrogen pulses through the upper divertor injection system resulted in immediate density increases with subsequent density decays after each valve closing. Due to the fast repetition rate, the density on average increased throughout the discharge, eventually leading to a radiative collapse at 4.7 s. A second goal of the same experiment was to trigger plasma detachment by the hydrogen injection. The gas pulses indeed triggered sudden drops of the



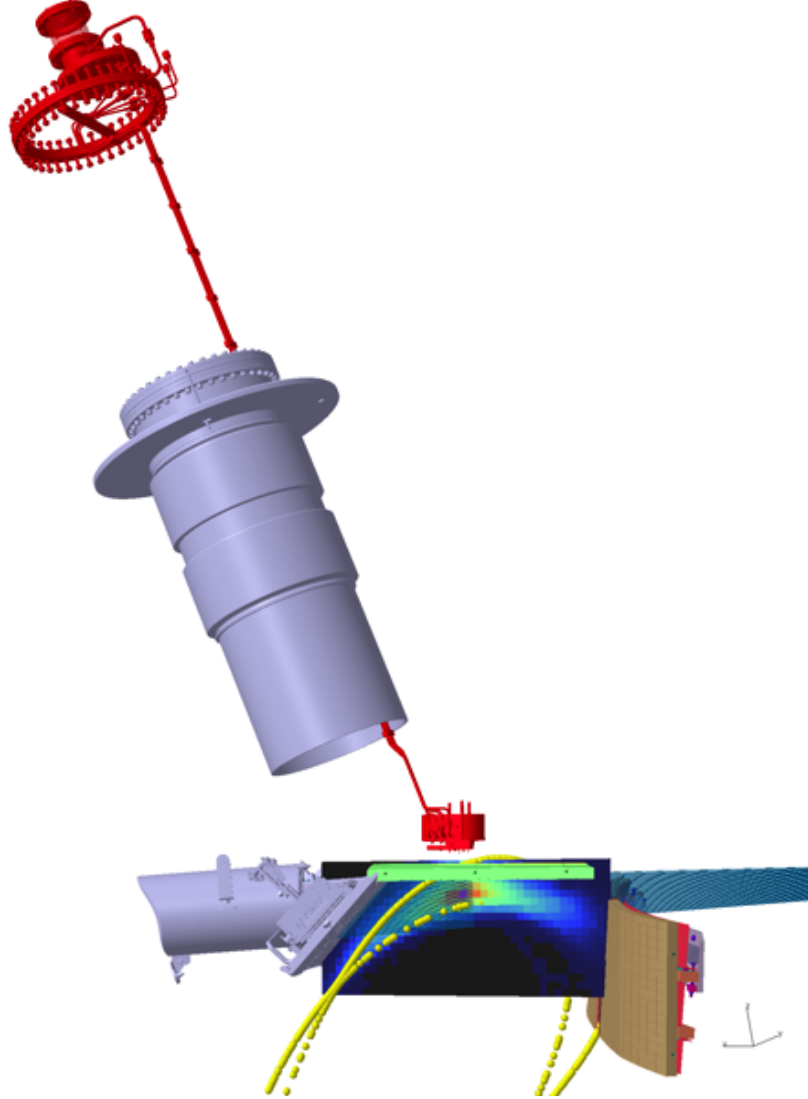


FIG. 9: CAD model of one of the divertor gas inlet systems (red). The cooling water, gas and cable lines are routed through a vacuum port that traverses the cryostat (grey). The piezo-valve box is attached to the backside of the horizontal divertor plate (green). An example simulation of He(I) radiation of injected tracer helium cloud is shown with a blue-green-red intensity color palette. The island chain defining the edge of the confinement region is shown in yellow .

heat loads to the divertors, shown in the bottom plot of Fig. 10. While at lower densities ( $\int n_e dl < 3.2 \times 10^{19} \text{ m}^{-2}$ ), the detached conditions were lost after closing the gas valve, the detachment was sustained even without any assist from the central gas injection system for higher densities ( $\int n_e dl > 3.2 \times 10^{19} \text{ m}^{-2}$ ).

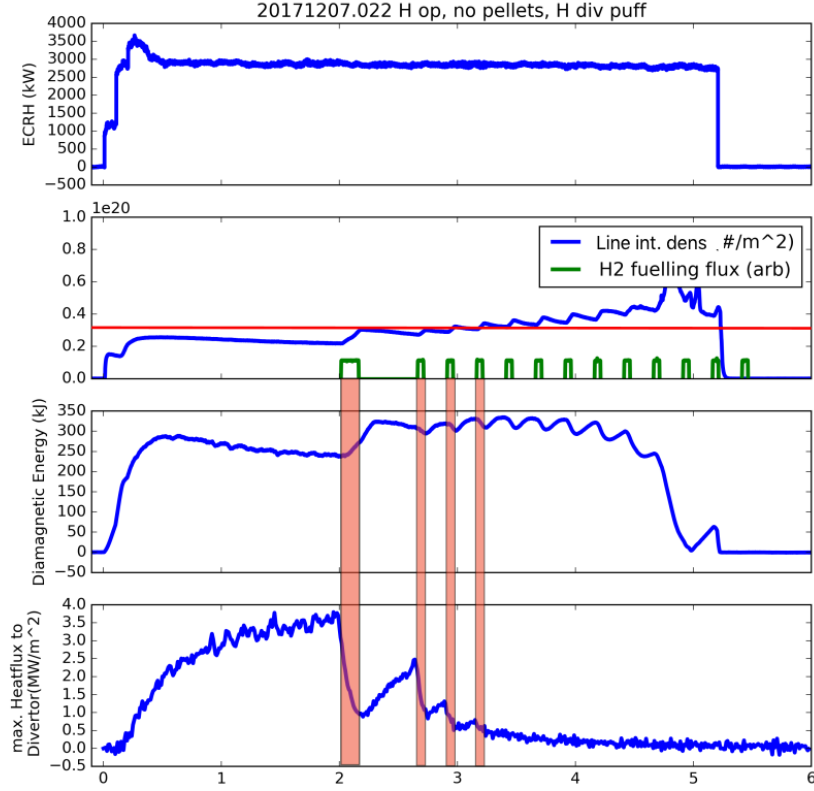


FIG. 10: Shown here are time traces of the ECRH heating power, the line-integrated electron density, the fuelled gas particle flux, the plasma diamagnetic energy and the maximum heat flux to the divertor module from which the gas was injected, for an experiment with the plasma being fueled and driven to detachment by the divertor gas injection system. Below the line-integrated density of  $3.2 \times 10^{19} \text{ m}^{-2}$ , the detached plasma conditions are sustained only transiently by the gas injection while above this threshold density the detachment was sustained until the end of the discharge. The heat flux patterns are shown in Fig. 11.

## X. STELLARATOR RECORD TRIPLE PRODUCT

During the relaxation period following intense pellet fueling, the plasma displayed high ion temperatures (appr. equal to the electron temperature), high beta values and improved confinement. This is not unexpected, since the ISS04 scaling predicts an improved energy confinement when the density is increased at constant heating power, and the higher density allows a closer collisional coupling of the electron and ion temperatures. During this time,

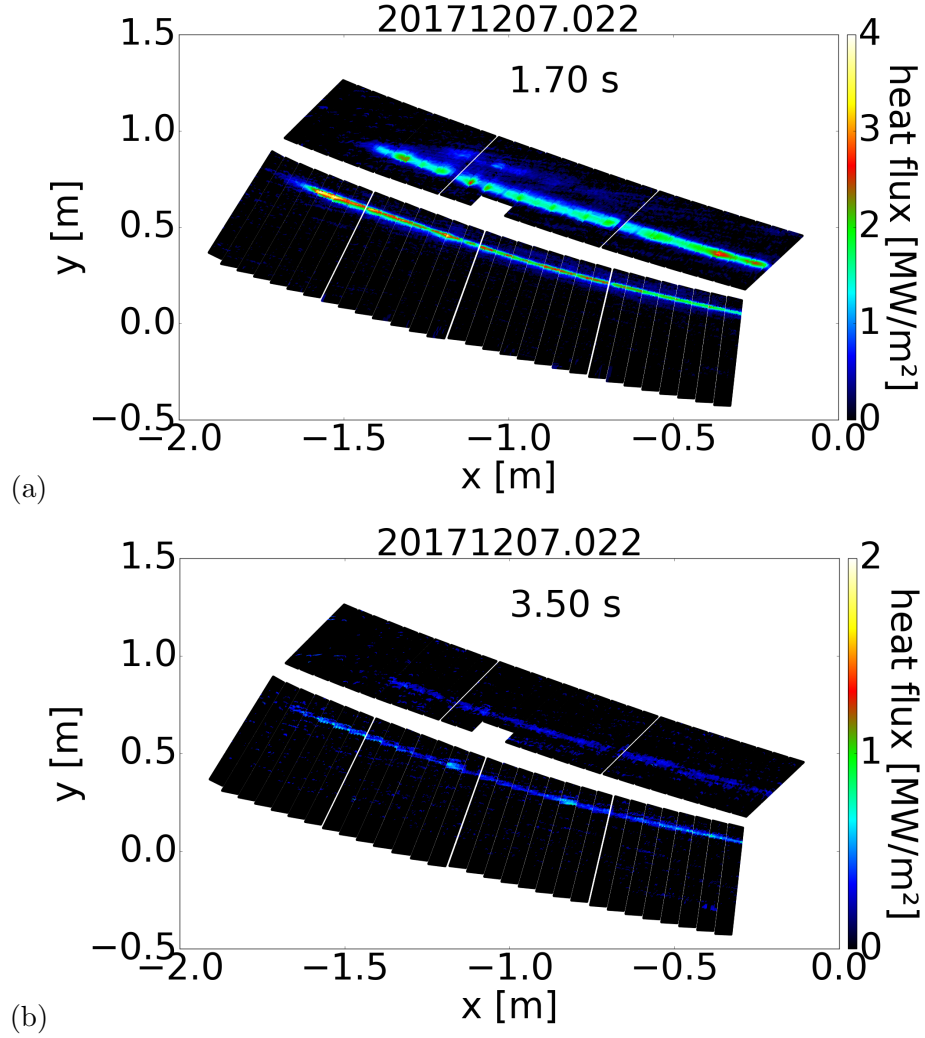


FIG. 11: Heat flux patterns for attached conditions (top) and detached (bottom) for the discharge fueled from the divertor gas inlet system. Note that the color scales are different between the two plots so that the heat load patterns are visible also during the detached phase.

a record triple product for stellarators was transiently achieved, Fig. 12. Figure 13 shows electron density profiles measured with the Thomson scattering system [41, 42], just before the pellet injection ( $t = 1.03$  s) and during the high-performance phase ( $t = 2.13$  s) for the mentioned discharge. Ion and electron temperature profiles for the high-performance time point are compared in Figure 14.

The ion temperature is obtained from the inversion of data from the X-ray imaging crystal spectrometer observing  $\text{Ar}^{+16}$  emission along multiple lines of sight [44]. The shown error

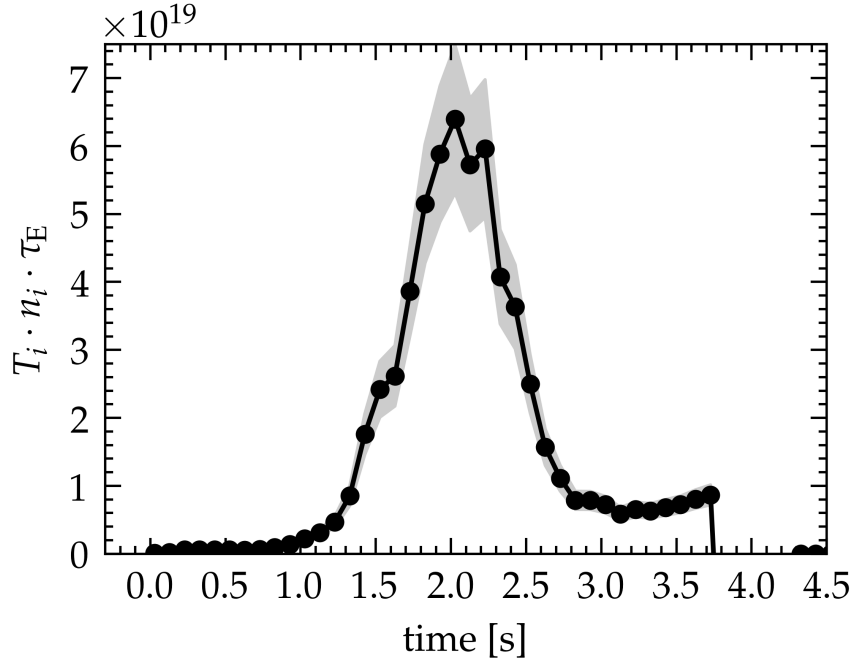


FIG. 12: The time evolution of the triple product for a P=5 MW shot is shown. As can be seen, this discharge was not stationary, and the previous stellarator/heliotron record from LHD of  $5.2 \times 10^{19} \text{ m}^{-3} \text{ keV s}$  was only exceeded for about 0.5 seconds.

bars are statistical and do not include possible systematic errors but we show results from two different inversion algorithms to exemplify possible systematic errors. In this discharges, the ion temperature closely approaches the electron temperature and is slightly above 3.5 keV in the core. The discrepancy between the two temperatures at the mid-radius is not clarified yet, but may indicate spatial mapping issues. At the same time as the high ion temperature is reached, the volume average beta approaches 1%, the central beta is above 3.5%, and the stored energy reaches 1.1 MJ as measured by diamagnetic loops. The plasma was heated with 5 MW of ECRH heating, the energy confinement time was 0.22 s, and this was held for only about that amount of time. Combined together these values, this is a triple product slightly above  $0.6 \times 10^{20} \text{ m}^{-3} \text{ keV s}$ . Here, the dilution of the hydrogen density due to impurities was taken into account as follows: The central  $Z_{eff}$  was estimated conservatively at 1.5, and carbon was assumed to be the dominant impurity. The core plasma was likely significantly cleaner than that during the high-performance phase, since it had been fueled intensely by hydrogen pellets. This could add about 10% to the achieved triple product, a correction which is still within the error bars indicated in grey in Fig. 12.

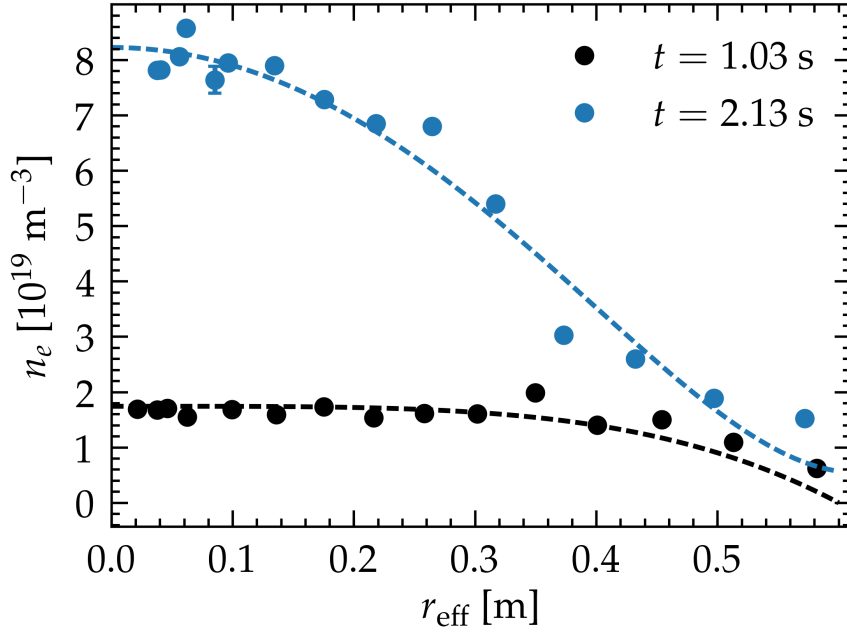


FIG. 13: The density profiles before pellet injection and around the time of the record triple product (shortly after pellet injection stopped) are shown. The density went up strongly during pellet fueling and there is a pronounced central peaking. The data were measured with the Thomson scattering system.

This is an increase of a factor of 8 over the best triple product achieved in OP1.1, which was  $0.08 \times 10^{20} \text{ m}^{-3} \text{ keV s}$  [2]. In Figure 15, we plot this data point in the Kikuchi diagram [2, 45]. It is worth noting that the W7-X record was made for an ion temperature of  $T_i \geq 3.5$  keV, as opposed to an ion temperature of 0.47 keV in LHD. Other parameters of the LHD record were  $\tau_E = 0.22 \text{ s}$ ,  $n_i = 5 \times 10^{20} \text{ m}^{-3}$ ,  $P=3.3 \text{ MW}$  [43]. This illustrates the points made in Section III, that high density, (more so than high heating power) is an effective way to increase the triple product in a given device.

It is expected in the OP1.2b phase that the divertor gas inlet system can help prolong the phases of high density and high performance significantly, but large increases in duration of high performance phases will likely need to wait until OP2, when the water-cooled divertor units and a continuous-injection pellet system will go into operation.

We also display these points in a  $n_i T_i \tau_E$  vs  $T_i$  plot, where the distance to D-T ignition conditions is more clearly displayed, Fig. 16. This graph shows that the W7-X results reported here are on par with medium-sized tokamaks, but also that there is still some distance to

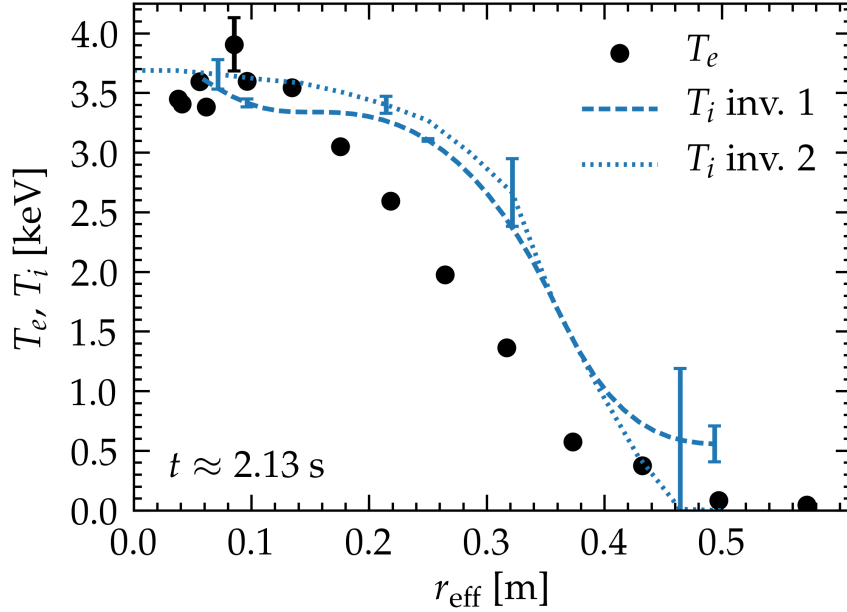


FIG. 14: The electron (black circles) and ion temperature profiles are shown around the time of the record triple product (shortly after pellet injection stopped). The electron temperature is determined by the Thomson scattering diagnostic. The apparent shift is likely unphysical, and may be related to uncertainties in the spatial calibrations of the two diagnostics. Two different inversion techniques were used for the  $T_i$  data, both using the XICS diagnostic signals.

the best results from DIII-D and ASDEX-Upgrade, which both are comparable in size and magnetic field strength to W7-X, but have operated for decades.

## XI. SUMMARY

The installation of a test divertor, as well as a number of other upgrades to W7-X, allowed for significant improvements in fusion performance. A factor of 8 increase in triple product was reached relative to that achieved in OP1.1. This is a new record triple product for stellarators. Densities around and above  $10^{20} \text{ m}^{-3}$  were reached, and heat-flux detachment was observed. The convective heat loads were deposited to a very large degree in the divertor, and the resulting strike lines were generally distributed as expected from code predictions. For attached divertor operation, the wetted area was large, indicating that an extrapolation to the expected higher heating powers in later operation phases will be compatible with the

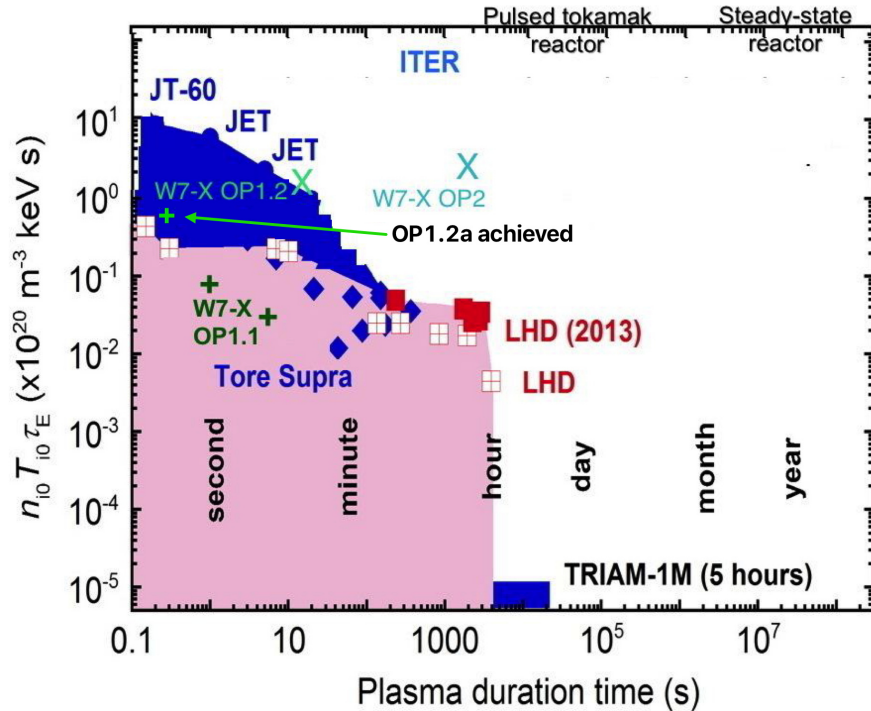


FIG. 15: Two important aspects of the progress towards a net energy producing fusion reactor are plotted here - the fusion triple product versus the length over which it was held. This figure is an updated version of the one in [2], originally based on work in [45]. +-signs indicate achieved values, X-s are code predictions from [2]. The newly achieved triple product record is indicated with the arrow.

steady-state water-cooled HHF divertor's technical specification of 10 MW/m<sup>2</sup>. It is also consistent with the expectation that the very long scrape-off layer connection lengths of the W7-X island divertor should result in very broad scrape-off layers .

## XII. ACKNOWLEDGEMENTS

This work has been carried out within the framework of the EUROfusion Consortium and has received funding from the Euratom research and training programme 2014-2018 under grant agreement No 633053. The views and opinions expressed herein do not necessarily reflect those of the European Commission. This work was funded in part by the Department

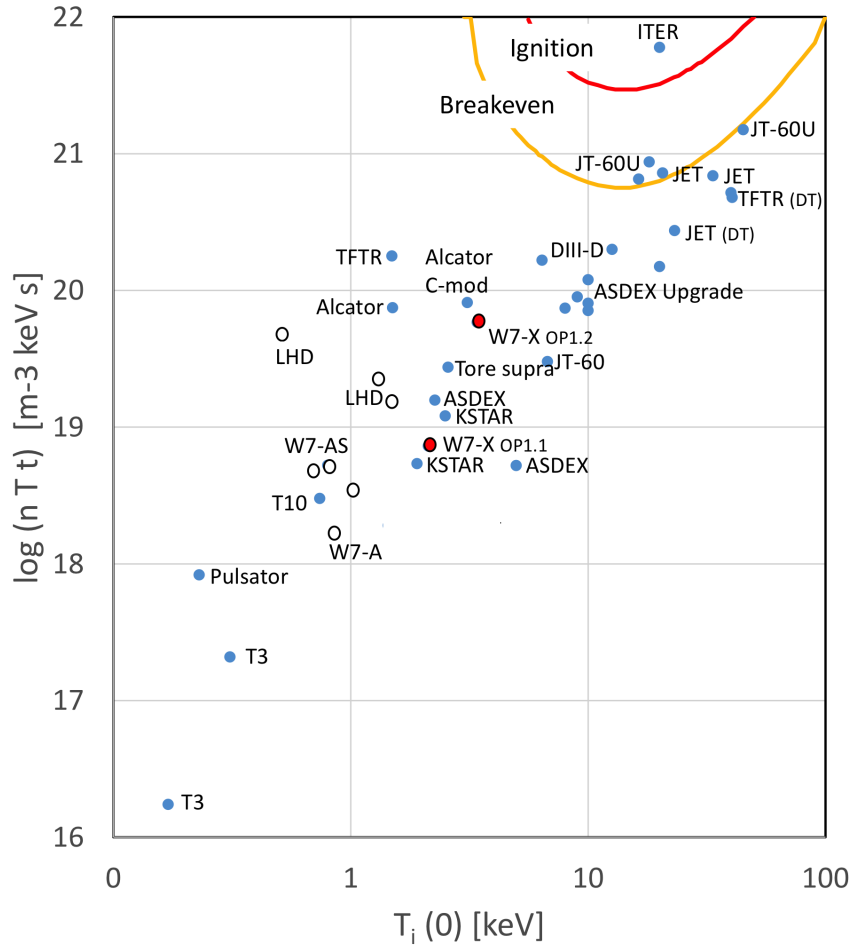


FIG. 16: Triple products versus ion temperatures are shown for a variety of experiments. The results from OP1.1 and OP1.2 in W7-X are shown in red, and compared to tokamaks (blue ) and stellarator/heliotron experiments (empty circles)

of Energy under Grant No. DE-SC0014210.

- 
- [1] C. Beidler, G. Grieger, F. Herrnegger, E. Harmeyer, J. Kisslinger, W. Lotz, H. Maassberg, P. Merkel, J. Nührenberg, F. Rau, J. Sapper, F. Sardei, R. Scardovelli, A. Schlüter, H. Wobig Physics and Engineering Design for Wendelstein VII-X. *Fusion Sci. Technol.* **17**, 148-168 (1990).
  - [2] T. Sunn Pedersen et al., *Physics of Plasmas* **24**, 055503 (2017)
  - [3] T. Klinger et al., *Plasma Physics and Controlled Fusion* **59**, 014018 (2017)



- [4] R. C. Wolf, C. Beidler, M. Beurskens, C. Biedermann, H.-S. Bosch, S. Bozhnikov, R. Brakel, A. Dinklage, Y. Feng, G. Fuchert, G. and O. Grulke, "Major results from the first plasma campaign of the Wendelstein 7-X stellarator", *Nuclear Fusion* **57**, 102020 (2017)
- [5] M. Hirsch, J. Baldzuhn, C. Beidler, R. Brakel, R. Burhenn, A. Dinklage, H. Ehmler, M. Endler, V. Erckmann, Y. Feng, Major results from the stellarator Wendelstein 7-AS. *Plasma Phys. Contr. Fusion* **50**, 053001 (2008).
- [6] M. Hirsch, A. Dinklage, A. Alonso, G. Fuchert, S. Bozhnikov, U. Höfel, T. Andreeva et al. (T. Sunn Pedersen) "Confinement in Wendelstein 7-X limiter plasmas." *Nuclear Fusion*, **57**, 086010 (2017)
- [7] H.-S. Bosch, R. Brakel, T. Braeuer, V. Bykov, P. van Eeten, J.-H. Feist, F. Füllenbach, M. Gasparotto, H. Grote, T. Klinger, H. Laqua, M. Nagel, D. Naujoks, M. Otte, K. Risse, T. Rummel, J. Schacht, A. Spring, T. Sunn Pedersen, R. Vilbrandt, L. Wegener, A. Werner, R. C. Wolf, J. Baldzuhn, C. Biedermann, H. Braune, R. Burhenn, M. Hirsch, U. Höfel, J. Knauer, P. Kornejew, S. Marsen, T. Stange, H. Trimino Mora, W7-X Team, "Final integration, commissioning and start of the Wendelstein 7-X stellarator operation", *Nuclear Fusion*, **57**, 116015 (2017)
- [8] A. Dinklage, C. D. Beidler, P. Helander, G. Fuchert, H. Maaßberg, K. Rahbarnia, T. Sunn Pedersen, Y. Turkin, R. C. Wolf, A. Alonso, T. Andreeva, B. Blackwell, S. Bozhnikov, B. Buttenschön, A. Czarnecka, F. Effenberg, Y. Feng, J. Geiger, M. Hirsch, U. Höel, M. Jakubowski, T. Klinger, J. Knauer, G. Kocsis, A. Krämer-Flecken, M. Kubkowska, A. Langenberg, H. P. Laqua, N. Marushchenko, A. Mollen, U. Neuner, H. Niemann, E. Pasch, N. Pablant, L. Rudischhauser, H. M. Smith, O. Schmitz, T. Stange, T. Szepesi, G. Weir, T. Windisch, G. A. Wurden, D. Zhang, the W7-X Team, *Nature Physics* **14**, p. 855-860 (2018)
- [9] R. S. Wolf et al., submitted to *Plasma Physics and Controlled Fusion* (2018)
- [10] T. Wauters, T. Stange, H.P. Laqua, R. Brakel, S. Marsen, D. Moseev, T. Sunn Pedersen, O. Volzke, S. Brezinsek, A. Dinklage and the W7-X team., Wall Conditioning by ECRH and GDC at the Wendelstein 7-X Stellarator, (43rd EPS Conf. on Plasma Physics. Leuven, Belgium, 2016) *ECA Vol. 40A*, P4.047 (2016)
- [11] Lawson, J. D. Some Criteria for a Power Producing Thermonuclear Reactor. *Proc. Phys. Soc. B* **70**, 6-10 (1957).

- [12] H. Yamada, J.H. Harris, A. Dinklage, E. Ascasibar, F. Sano, S. Okamura, J. Talmadge, U. Stroth, A. Kus, S. Murakami, et al., *Nuclear Fusion* **45** 1684 (2005)
- [13] C. Nührenberg, Free-boundary ideal MHD stability of W7-X divertor equilibria, *Nucl. Fusion* **56** 076010 (2016)
- [14] M. Greenwald, Density limits in toroidal plasmas, *Plasma Phys. Control. Fusion* **44** (2002) R27-R53
- [15] F. Troyon, R. Gruber, H. Saurenmann, S. Semenzato, and S. Succi, MHD-Limits to Plasma Confinement, *Plasma Physics and Controlled Fusion* **26**, p. 209 (1984)
- [16] H Yamada et al *Plasma Phys. Control. Fusion* **49**, B487 (2007)
- [17] S. Sudo, Y. Takeiri, H. Zushi, F. Sano, K. Itoh, K. Kondo and A. Iiyoshi, Scalings of energy confinement and density limit in stellarator/heliotron devices, *Nuclear Fusion* **30**, 11 (1990)
- [18] P. Zanca, F. Sattin, D. F. Escande, G. Pucella and O. Tudisco, A unified model of density limit in fusion plasmas, *Nucl. Fusion* **57** 056010 (2017)
- [19] G. Fuchert et al., Proc. 23 Europ. Conf. on Circuit Theory and Design (2017, Catania, Italy), 2017
- [20] A. Peacock, H. Greuner, F. Hurd, J. Kißlinger, R. König, B. Mendelevitch, R. Stadler, F. Schauer, R. Tivey, J. Tretter, C. von Sehren, M. Ye, Progress in the design and development of a test divertor (TDU) for the start of W7-X operation *Fusion Eng. Des.* **84** 1475 8 (2009)
- [21] H. Renner, D. Sharma, J. Kißlinger, J. Boscary, H. Grote, R. Schneider Physical aspects and design of the Wendelstein 7-X Divertor, *Fusion Sci. Technol.* **46** 318 (2004)
- [22] Y Feng et al *Plasma Phys. Control. Fusion* **53** 024009 (2011)
- [23] S. Bozhenkov, J. Geiger, M. Grahl, J. Kißlinger, A. Werner, R. C. Wolf, Service oriented architecture for scientific analysis at W7-X. An example of a field line tracer. *Fusion Eng. and Design* **88** p. 2997-3006 (2013)
- [24] T. Sunn Pedersen, M. Otte, S. Lazerson, P. Helander, S. Bozhenkov, C. Biedermann, T. Klinger, R. C. Wolf, H. -S. Bosch, and the Wendelstein 7-X Team, Confirmation of the topology of the Wendelstein 7-X magnetic field to better than 1:100,000, *Nature Communications* **7** 13493 (2016)
- [25] M.W. Jakubowski, et al., *Rev. Sci. Instruments*, accepted for publication
- [26] B. Sieglin, et al., *Rev. Sci. Instrum.* **86**, 113502 (2015).

- [27] B. Sieglin, et al., Plasma Phys. Control. Fusion **58**, 055015 (2016).
- [28] M. Dibon, Master-Thesis, Entwicklung und Verbesserung eines Blower Gun Pellet Injektors für die Anwendung in thermonuklearen Fusionsanlagen, Technical University of Munich, Max Planck Institute for Plasma Physics (2014)
- [29] P. Lang et al.: High-Efficiency Plasma Refuelling by Pellet Injection from the Magnetic High-Field Side into ASDEX Upgrade. Phys. Rev. Lett. **79**, 1487, (1997)
- [30] K. Rahbarnia et al , Nucl. Fusion **58** 096010 (2018)
- [31] D. Zhang, et al., First observation of a stable highly-radiative divertor regime at stellarator W7-X, 45th EPS Conference on Plasma Physics, Prag (2018) O3.103
- [32] T Wauters, et al., Wall conditioning throughout the first carbon divertor campaign on Wendelstein 7-X, submitted to Nuclear Materials and Energy (2018)
- [33] U. Wenzel et al., Nucl. Fusion **55** 013017 (2015)
- [34] M. Krychowiak et al., Rev. Sci. Instrum. **87**, 11D304 (2016).
- [35] T. Barbui, et al, 45th EPS Conference on Plasma Physics; 2018, Prague, Czech Republic, P4.1018.
- [36] M. Krychowiak et al, Plasma Phys. Control. Fusion **53** (2011) 035019.
- [37] F. Effenberg et al., Investigation of 3D effects on heat fluxes in performance optimized island divertor configurations at Wendelstein 7-X, submitted to Nuclear Materials and Energy, Proceedings of 23rd International Conference on Plasma Surface Interactions in Controlled Fusion Devices (PSI-23) 2018.
- [38] V.R. Winters, et al, Poster: EPS 45th conference on Plasma Physics; 2018; Prague, Czech Republic.
- [39] L. Stephey, Phys. Plasmas **25**, 062501 (2018).
- [40] R. König et al, in preparation for PRL.
- [41] E. Pasch, M. N. A. Beurskens, S. A. Bozhnikov, G. Fuchert, J. Knauer, R. C. Wolf, and W7-X Team, The Thomson scattering system at Wendelstein 7-X, Review of Scientific Instruments **87**, 11E729 (2016); <https://doi.org/10.1063/1.4962248>
- [42] S.A. Bozhnikov, M. Beurskens, A. Dal Molin, G. Fuchert, E. Pasch, M.R. Stoneking, et al. Journal of Instrumentation **12** P10004 (2017)
- [43] T. Morisaki, private communication (2018)

- [44] A. Langenberg et al., Nucl. Fusion **57** 086013 (2017)
- [45] Fig. 3.16 and Appendix of Chapter 3 , in M. Kikuchi, M. Azumi, Frontiers in Fusion Research II (Introduction to Modern Tokamak Physics), ISBN 978-3-319-18905-5, Springer Verlag (2015)